Journal of Structural Biology 174 (2011) 1–10

Contents lists available at ScienceDirect

Journal of Structural Biology

journal homepage: www.elsevier.com/locate/yjsbi

Review

Precise beam-tilt alignment and collimation are required to minimize the phase error associated with coma in high-resolution cryo-EM

Robert M. Glaeser [a,*], Dieter Typke [a], Peter C. Tiemeijer [b], James Pulokas [c], Anchi Cheng [c]

[a] Life Sciences Division, Lawrence Berkeley National Laboratory, University of California, Berkeley, CA 94720, USA
[b] FEI Company, P.O. Box 80066, 5600 KA Eindhoven, The Netherlands
[c] National Resource for Automated Molecular Microscopy, The Scripps Research Institute, La Jolla, CA 92037, USA

ARTICLE INFO

Article history:
Received 17 May 2010
Accepted 15 December 2010
Available online 21 December 2010

Keywords:
Beam alignment
Coma
Phase error

ABSTRACT

Electron microscopy at a resolution of 0.4 nm or better requires more careful adjustment of the illumination than is the case at a resolution of 0.8 nm. The use of current-axis alignment is not always sufficient, for example, to avoid the introduction of large phase errors, at higher resolution, due to axial coma. In addition, one must also ensure that off-axis coma does not corrupt the data quality at the higher resolution. We particularly emphasize that the standard CTF correction does not account for the phase error associated with coma. We explain the cause of both axial coma and the typically most troublesome component of off-axis coma in terms of the well-known shift of the electron diffraction pattern relative to the optical axis that occurs when the illumination is not parallel to the axis. We review the experimental conditions under which coma causes unacceptably large phase errors, and we discuss steps that can be taken when setting up the conditions of illumination, so as to ensure that neither axial nor off-axis coma is a problem.

1. Introduction

Thin biological samples, when prepared for electron microscopy as unstained, frozen-hydrated specimens, can be modeled as weak phase objects. Images of such specimens must be recorded with a substantial amount of defocus in order to generate adequate contrast at low spatial frequencies. One must then apply a systematic correction to the higher-frequency Fourier components of the image in order to compensate for the resulting oscillations in the phase-contrast transfer function (CTF), $\sin \gamma(s)$, where $\gamma(s)$ is the amount by which the phase of the electron wave-front at the back focal plane of the objective lens deviates relative to the phase of a converging spherical wave. One must also take account of an overall envelope of the contrast transfer function that occurs due to beam-induced movement (Henderson and Glaeser, 1985; Typke et al., 2007), partial spatial and temporal coherence (Frank, 1973; Frank, 2006; Wade and Frank, 1977), and the modulation transfer function (MTF) of the detector. For simplicity, we do not consider the envelope of the CTF in this review; suffice it to say that one can compensate for the envelope by empirical sharpening of the density map (Fernandez et al., 2008).

As the resolution increases, small amounts of beam tilt can result in a significant amount of coma, an image aberration that is often ignored in cryo-EM. Unlike the familiar effects of defocus and spherical aberration, the effect of coma generally cannot be represented in terms of a $\sin \gamma(s)$ contrast transfer function. Instead, both imperfectly aligned illumination and imperfectly collimated illumination can cause a large (e.g. greater than 45°), azimuthally varying phase error in the computed Fourier transform. In addition, increasing amounts of coma occur as one considers image points that are farther and farther from the optical axis, even when the illumination is everywhere parallel to the optical axis.

Although computational correction of the phase error introduced by coma requires the determination of only a small number of parameters, it is more challenging to determine the values of these parameters from images of single particles than it was for images of 2-D crystals (Henderson et al., 1986). As a result, it is worthwhile to ensure that there is as little coma as possible during data collection. The two approaches are not mutually exclusive, of course, and the development of successful software tools for correction of the systematic phase error due to (residual) coma in single-particle EM would clearly be of great value.

Structures of randomly dispersed macromolecular particles (as well as 2-D crystals and helical assemblies) are now being realized at resolutions of 0.4 nm and better (Chen et al., 2009; Cong et al., 2010; Jiang et al., 2008; Ludtke et al., 2008; Wolf et al., 2010; Yu et al., 2008; Zhang, 2010; Zhang et al., 2008; Zhou, 2008). It thus

* Corresponding author. Address: 363B Donner Laboratory, Lawrence Berkeley National Laboratory, University of California, Berkeley, CA 94720, USA. Fax: +1 510 486 6488.
E-mail address: rmglaeser@lbl.gov (R.M. Glaeser).

1047-8477/$ - see front matter © 2011 Elsevier Inc. All rights reserved.
doi:10.1016/j.jsb.2010.12.005

seems timely to review (1) why coma introduces phase errors (at high resolution) that are not accounted for by the "sin $\gamma(s)$" model of contrast transfer, (2) when and why (in practical terms) such phase errors become important; and (3) what must be done to minimize the effects of coma. In addition to reviewing the theoretical background needed to understand these issues, we provide specific examples of the extent to which the illumination can be condensed at the specimen plane, for a given C2-aperture size, without introducing an excessive phase error due to coma.

To provide insight regarding the origin of the phase error, we use the familiar Abbe theory (model) of image formation to explain that coma occurs when the center of the electron-scattering pattern does not coincide, at the back focal plane, with the center of the inversion-symmetric phase-distortion function, $\gamma(s)$, the familiar form of which is defined in Eq. S1. We explain coma as being due to a tilt-induced shift of the electron diffraction pattern relative to the (axial) coma-free optical axis, as we believe that this approach will be physically more understandable for most practitioners of cryo-EM than is the traditionally used power-series expansion, the coefficients of which correspond to progressively higher-order lens aberrations [see, for example, pp197ff of Rose (2009)]. In order to further simplify the main text of our review, we use Footnotes – which readers need not consult before continuing – to expand upon various points.

2. Fundamental background for a discussion of coma

2.1. Symmetry origins and a practical definition of what is meant by the phrase "optical axis"

In a familiar idealization, one can imagine the existence of a unique optical axis for the objective lens. In the case of a thin, glass (i.e. light-optical) lens, for example, the optical axis is perpendicular to the plane of the lens and passes through the center of rotational symmetry of the lens. According to this concept (definition) of the optical axis, there is only one point at which the optical axis passes through the specimen, i.e. only one point of the specimen is on the optical axis. In electron optics, on the other hand, it would be difficult to identify the location of the optical axis, defined in this way, for several reasons, not the least being that it is hardly possible to produce a lens that has perfect rotational symmetry.

In more practical terms, any point of the specimen that happens to be at the middle of the field of view can actually serve as one point on what we choose to call "the optical axis", even if that point is not on the idealized optical axis that was imagined above. As we discuss more fully below, a beam-tilt angle can be found such that the image coma becomes negligible for the chosen point in the specimen. Once this unique tilt angle has been found, the position of the unscattered electron beam, focused in the back focal plane of the objective lens, also lies on this "optical axis"[1]. To speak more carefully, one should refer to this axis as the coma-free axis for a given point in the specimen, but in practice one normally refers to the axis defined by coma-free alignment as being "the optical axis", i.e. as if it were unique. We elaborate further on this point, below, especially in Footnotes (1) and (2).

[1] A single ray that passes through the center of a thin lens is not deflected by the lens, even when the ray is no longer normal to the plane of the lens. Each member of a small bundle of rays surrounding (and parallel to) the one that passes through the center of the lens is deflected by the lens, however, and thus all members of the bundle are focused onto the axis that is defined by any chosen point in the specimen and the center of the lens. In effect, the search for a beam-tilt angle that eliminates axial coma is a search for the beam-tilt angle that puts an unscattered ray through the center of the lens.

Once the tilt angle of the illumination has been set to the coma-free condition, the point where the optical axis passes through the back focal plane serves as the origin of the coordinate system for both the structure factor, $F(\boldsymbol{s})$ and the phase-distortion function, $\gamma(s)$. The coma-free axis (for the particular point in the specimen that is being considered) remains fixed relative to the pole pieces of the objective lens when the illumination is tilted. At the same time, however, the origin of the coordinate system of the structure factor, $F(\boldsymbol{s})$ now shifts relative to its previous position when the beam-tilt angle is changed. Since it is only the relative shift between the center of symmetry of $\gamma(\boldsymbol{s})$ and the center of symmetry of $F(\boldsymbol{s})$ that produces the coma that we are concerned with, however, one can just as well adopt a convention in which the structure factor remains stationary while the center of symmetry of the phase-distortion function moves when the illumination is tilted. This latter convention is actually the more convenient one to adopt from a mathematical point of view, since we will want to use the center of symmetry of the structure factor as the origin of our coordinate system when we calculate the image wave function by taking the inverse Fourier transform of the wave in the back focal plane.

2.2. Image formation when the center of symmetry of the structure factor and the center of symmetry of the phase-distortion function do not coincide

The mathematical form of the standard phase-contrast transfer function is well known, and derivations are given in various reference books (Frank, 2006; Glaeser et al., 2007). A crucial, but not often mentioned assumption that is used in the standard derivations is that the incident beam is parallel to the optical axis. While we do not repeat the details here, we present an alternative form of the derivation in the supplementary material. This form of the derivation emphasizes that the image intensity is, for a weak phase object, the sum of sinusoidal fringes that are produced by the interference of individual scattered beams with the unscattered beam. In this form of the derivation it is apparent that the phase of each such sinusoidal fringe is shifted by the phase-distortion function, $\gamma(s)$. As we emphasize in connection with Eq. (S9), these phase shifts result in the familiar, $\sin\gamma(s)$, CTF through a convenient algebraic simplification, but only when the amount of the phase shift is the same for a diffracted beam and its Friedel mate.

When the crucial assumption of inversion-symmetric phase shifts is not satisfied with sufficient precision, the algebraic consequences become more complicated, of course. Following the same approach that is used to derive Eq. (S8), the image intensity for each Fourier component in a given specimen can again be described as the superposition of two distinct two-beam interference fringes, one of which is produced by a given scattered beam and the other of which is produced by its Friedel mate. Since the origin of the phase-distortion function no longer coincides with the origin of the structure factor, however, the values of the phase shifts, $\gamma(s)$, are no longer equal in magnitude for the two scattered beams. To emphasize this point, we show schematically, in Fig. 1, how displacing the centers of symmetry of the two functions by a vector $\boldsymbol{s}'$ results in the amount of the phase distortion being different for a scattered beam and for its Friedel mate.

The resulting expression for the image intensity, corresponding to the one derived in equation S8, is now given by

$$I_{\text{Friedel mates}}(\boldsymbol{x}) = 1 + 2|F(\boldsymbol{s})|\cos\left\{2\pi\boldsymbol{s}\cdot\boldsymbol{x} + \alpha(\boldsymbol{s}) - \gamma(\boldsymbol{s}+\boldsymbol{s}') + \frac{\pi}{2}\right\} + 2|F(\boldsymbol{s})|\cos\left\{2\pi\boldsymbol{s}\cdot\boldsymbol{x} + \alpha(\boldsymbol{s}) + \gamma(\boldsymbol{s}-\boldsymbol{s}') - \frac{\pi}{2}\right\}, \quad (1)$$

where $\boldsymbol{s}$ is the spatial frequency, $F(\boldsymbol{s})$ is the electron-scattering structure factor of the object, and $\alpha(\boldsymbol{s})$ is the phase of the structure

factor. See also the steps in the derivation of Eq. (S8) for the definition of this notation. An important feature that appears in Eq. (1), which was not present in Eq. (S8), is the fact that the value of the phase distortion, $\gamma(\boldsymbol{s})$, that is applied to a Fourier component of spatial frequency, $\boldsymbol{s}$, is now dependent upon the amount of beam tilt, expressed in terms of a spatial frequency, $\boldsymbol{s}'$. In other words, the amount of phase shift is no longer the same for a given scattered beam and for its Friedel mate.

3. Axial coma

3.1. Physical description of axial coma

Axial coma is an image aberration that is introduced when the illumination is not parallel to the optical axis of the objective lens[2]. Since, as is indicated schematically in Fig. 1, the origin of the phase-distortion function is shifted relative to the origin of the structure factor when the illumination is not parallel to the optical axis, the respective phase shifts at spatial frequencies $\boldsymbol{s}$ and $-\boldsymbol{s}$ (in the coordinate system of the structure factor), are no longer the same for the pair of interference fringes that is generated by Friedel mates $F(\boldsymbol{s})$ and $F(-\boldsymbol{s})$. As a result, the trigonometric identity that was used to factor out a term dependent on the phase shifts, $\gamma(s)$, is no longer applicable, and thus the image intensity can no longer be described in terms of the familiar "sin $\gamma(s)$ CTF".

When the beam tilt is small, the result can nevertheless be approximated as consisting of the familiar focus-dependent image shift[3] together with three additional effects (Smith et al., 1983; Typke and Dierksen, 1995; Zemlin et al., 1978). These three effects are the introduction of an excess increment of defocus[4],

$$\Delta z_{\text{effective}} - \Delta z_{\text{no beam tilt}} = -2C_s\theta^2; \tag{2}$$

the introduction of excess astigmatism,

$$A_{\text{beam tilt}} = C_s\theta^2, \tag{3}$$

which, in general, is in a direction different from the astigmatism (if any) that exists without beam tilt; and the introduction of axial coma, which produces an azimuthally varying phase error that increases in value as the third power of the resolution,

$$\text{Phase error} = 2\pi\theta C_s\lambda^2 s^3(\hat{\boldsymbol{\theta}}\cdot\hat{\boldsymbol{s}}), \tag{4}$$

where, $\hat{\boldsymbol{\theta}}$ is a unit vector in the direction of the beam tilt, and $\hat{\boldsymbol{s}}$ is a unit vector in the direction of the spatial frequency vector.

Before continuing, it is worthwhile to acknowledge that what is meant by the phrase "beam tilt" can be ambiguous or confusing. If we assume, for example, that the second condenser lens is overfocused, thereby producing a demagnified image of the source at a point above the specimen, then – as is illustrated in Fig. 2 – the angle of illumination at any given point on the specimen can be described in terms of three different angles (Christenson and Eades, 1988).

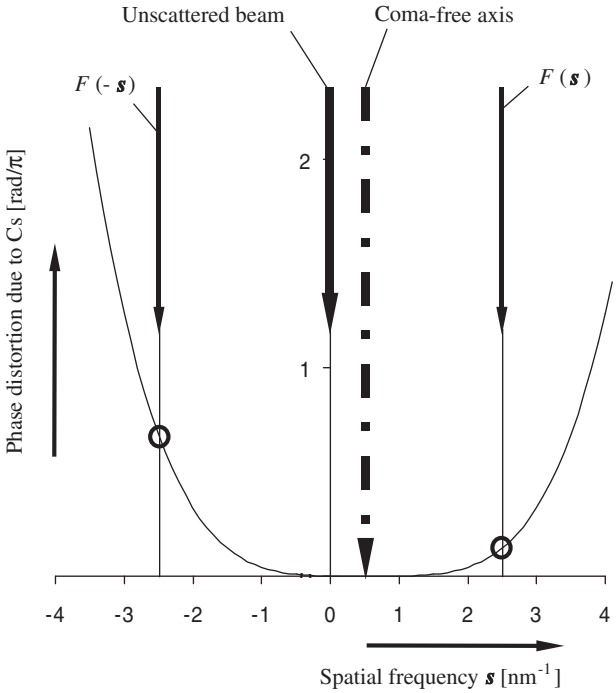

Fig. 1. Illustration of the fact that the phase-distortion function, $\gamma(\boldsymbol{s})$, no longer has the same value on opposite sides of the scattered wave when the incident illumination is tilted relative to the optical axis of the objective lens. For simplicity, only the contribution from spherical aberration is shown in this figure, since – for small tilt angles – the contribution from defocus (if any) causes only a shift (displacement) of the entire image. As is shown in this figure, beam-tilt shifts the center of the diffraction pattern relative to the optical axis, thus breaking the inversion symmetry that is required in order for the image to be accurately described in terms of the familiar phase-contrast transfer function, sin γ. The curve shown here was calculated for 300 keV electrons, assuming C_s = 2.2 mm, zero defocus, and a beam tilt of 1 mrad.

The necessarily finite size of the focused beam crossover makes it impossible for the illumination to be perfectly parallel at any point on the specimen, as is indicated in Fig. 2A. Instead, this "virtual source" of electrons subtends an angle α (which is not to be confused with the phase of the structure factor, for which we have used the same symbol in Eq. (1) and in Eq. (S6)) that is the same for each point on the specimen. The angle α determines the degree of spatial coherence of the illumination, which in turn contributes to the envelope function of the contrast transfer function. As was indicated previously, however, we are not concerned here with the role of the envelope function.

Ignoring the small fan of illumination angles associated with the finite source size, the angle θ shown in Fig. 2B corresponds to what is normally meant when one refers to the beam tilt. This is, in fact, the only tilt angle that is referred to when discussing axial coma, the topic of this section.

One other beam-tilt angle is shown in Fig. 2C, however. Different points on the specimen will generally be illuminated at different angles, β, the value of which depends upon the distance between the demagnified virtual image of the source and the specimen, a point that we take up more fully in the section on off-axis coma that follows. This form of beam tilt also causes coma, but now the beam-tilt angle – and thus the amount of coma – depends upon how far a given position within the specimen is from the optical axis. However, as we explain in the section on off-axis coma, the beam tilt that is characterized by the angle β is only one factor that gives rise to off-axis coma.

[2] As we stated above, any position within the field of view can be regarded as being the position of the optical axis, once the beam tilt is adjusted to produce a coma-free image at that point. As a result, there is an infinite number of coma-free axes, one for each point in the field of view. For conceptual simplicity, however, it is common to speak as if the optical axis of the lens could be defined uniquely. As was pointed out by Zemlin et al. (1978), physical alignment of the lens pole pieces (or equivalently, the use of deflection coils to shift the image by an appropriate amount) can make the voltage-axis center coincide with the coma-free image point, and this additional alignment step does, indeed, serve to define a unique optical axis.

[3] The image shift is actually due to a tilt-associated phase "error" that occurs in double-sideband images (in addition to that given in Eq. (4)), which increases linearly with resolution and which is proportional to the amount of defocus. This image-shift effect is what is exploited when an intentional beam tilt is used to measure the amount of defocus (Koster and de Ruijter, 1992).

[4] We use the convention throughout that Δz is taken to be positive for underfocus.

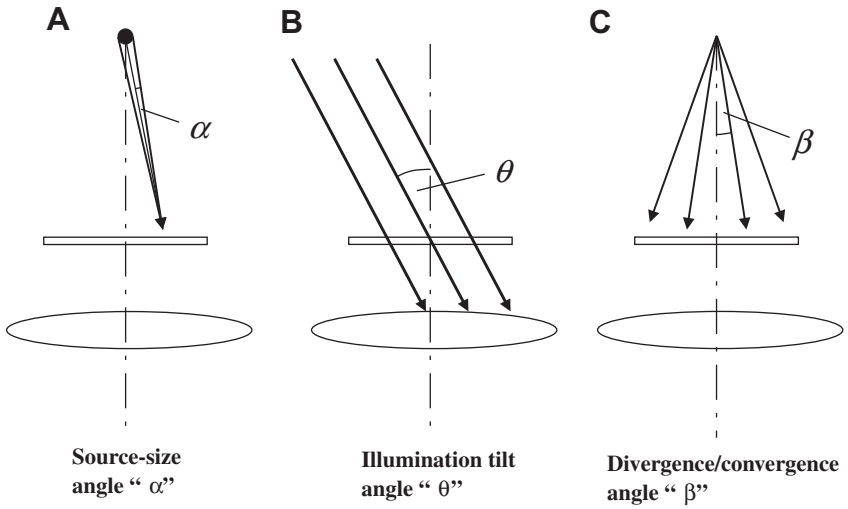

Fig. 2. Illustration of three physical effects that can cause the incident illumination to be tilted relative to the optical axis of the objective lens. A fourth effect, not shown here but explained in the text, results in an azimuthal tilt of the illumination, due to the spiral trajectories of electrons within the magnetic field of the objective lens. As is shown in the figure, the angles α and β describe the direction of a ray relative to the mid-point of a distribution; the same symbols are also used to refer to the half-angle of the distribution. (A) A given point on the specimen is illuminated by a finite "source" of electrons, i.e. the final beam crossover that is formed above the specimen. As a result, the illumination angle varies over a small range, with half-angle α. Although the necessarily finite source-size limits the spatial coherence of the illumination, it is not normally a consideration when discussing coma. (B) Assuming that the illumination can be approximated as being perfectly parallel, the direction of the beam may still be tilted by an angle, θ, relative to the optical axis. (C) Assuming that the final beam crossover can be approximated as a point source, the illumination reaching the specimen is nevertheless either a diverging spherical wave (as is shown in this panel) or a converging spherical wave. As a result, the local tilt angle, β, varies continuously over the illuminated area. As is explained in the text, the maximum value of β depends upon the position of the beam crossover relative to the front focal plane of the objective-lens "pre-field", and β is zero only when the illumination is focused exactly onto the front focal plane of the pre-field lens.

3.2. When is axial coma important?

As is shown in Eq. (4), the phase error due to coma increases steeply (i.e. as the third power) with the resolution (expressed as the spatial frequency, s). As a result, coma may cause a negligible effect up to a given resolution (say 0.8 nm), but at the same time it may cause the phases to be essentially random at only twice that resolution (say 0.4 nm). The parameters that determine whether axial coma is important, for which the user has experimental control, are the beam tilt, which we emphasize in the discussion below, and the electron wavelength. The wavelength-squared dependence of the phase error is actually quite significant. All else being equal, for example, the phase error is reduced by a factor of $\sim$2.2 when going from an electron energy of 100 keV to 200 keV, and it is further reduced by a factor of $\sim$1.6 when going from 200 keV to 300 keV.

Another important point to make is that the other two effects of beam tilt, i.e. the introduction of excess defocus and excess astigmatism, actually remain negligible at the point when the phase error due to axial coma first becomes too large to ignore. Referring to Eqs. (2) and (3), respectively, and assuming $C_s = 2.5$ mm and $\lambda = 2$ pm (i.e. electron energy = 300 keV), a beam tilt of 1 mrad introduces an excess defocus of only 5 nm and an excess astigmatism that is only half that value, while the maximum phase error is already $\sim$56° at a resolution of 0.4 nm. Since the values of the accelerating voltage and the coefficient of spherical aberration, C_s, vary from one microscope design to another, the reader should use Eqs. (2)–(4) to calculate the values that apply to their respective research instruments.

Because the excess defocus and the excess astigmatism are relatively insensitive to beam tilt, alignment of the incident beam to the current axis of the objective lens is fully effective as a way to reduce these two effects to negligibly small values. At the same time, however, one must be aware that current-axis alignment is generally not accurate enough to ensure high-quality phase information at high resolution. Instead, it is important to use the "coma-free" alignment method described below to ensure that the illumination is as parallel to the optical axis as possible.

3.3. What can be done to prevent axial coma?

Two alternatives can be recommended for performing (axial) coma-free alignment. A fast but somewhat qualitative procedure is to slowly switch ("wobble") the beam tilt back and forth by plus and minus $\sim$10 mrad, first in the x-direction and then in the y-direction, while viewing the image on the fluorescent screen (or with a video-rate camera). The amount of beam tilt is adjusted (as the tilt is wobbled) until the image that is seen with a plus tilt angle is indistinguishable from that seen with a minus tilt angle. A more quantitative procedure is to generate a tableau of CTF patterns corresponding to a systematic pattern of beam tilt, as was used by Zemlin et al. (1978). If the first such tableau shows visible asymmetry from left to right or from top to bottom, the amount of beam tilt in the "aligned" position is changed and a new tableau is generated. This process is continued until the tableau is made as symmetric in appearance as is possible. An example is presented in Fig. 3, where the five-panel tableau that was initially obtained after current-axis alignment is shown in Fig. 3A, while Fig. 3B shows the tableau that was obtained after optimizing the amount of beam tilt in the "aligned" position.

In addition to using one of the above methods of coma-free alignment, it is important to first adjust the alignment pivot-points in both the x and y directions such that translating the beam does not introduce a beam tilt, and such that applying a beam tilt does not cause a significant beam translation. Some types of microscopes provide menu-driven instructions for adjusting the pivot points. When that is not the case, it is advisable to ask the local service engineer for instruction on how to do the required adjustment of pivot points.

4. Off-axis coma

4.1. Physical explanation of the effect

The magnitude of the local beam-tilt angle increases linearly with the distance from the coma-free axis when the illumination

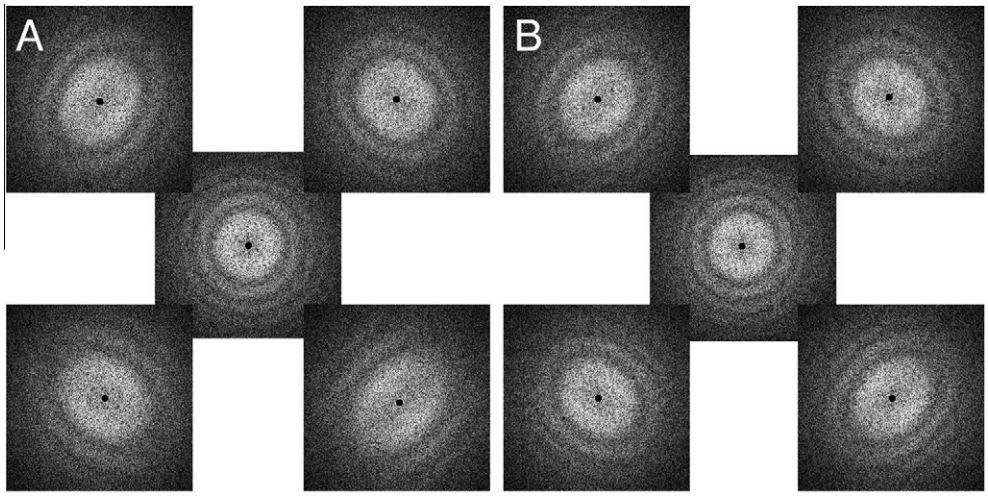

Fig. 3. A comparison of the tableau of FFTs obtained after current-axis alignment to the tableau obtained after (nearly) coma-free alignment. (A) FFT tableau obtained after current-axis alignment. The center panel shows the FFT of an image recorded without applying an additional beam tilt, while the panels on the four corners show the FFTs for images recorded after applying additional beam tilts of approximately ± 5 mrad in the x and y directions, respectively. The fact that the astigmatism is slightly different for "plus" versus "minus" tilt angles demonstrates that the beam direction after performing current-axis alignment (i.e. in the central panel) is not parallel to the coma-free axis. (B) FFT tableau after performing coma-free alignment, i.e. after adjusting the beam-tilt angle so as to make the defocus and astigmatism as similar as possible for symmetrical beam tilts in the *x* and *y* directions, respectively.

is divergent (or, alternatively, convergent) at the plane of the specimen, as it is shown to be in Fig. 2C. The coma that results from this off-axis beam tilt is directed radially, and it has the same magnitude for all points in the specimen that are a given distance from the coma-free axis. This contribution to off-axis coma is identical to the coma that occurs in a glass lens, and it is often referred to as isotropic coma. Failure to ensure that the off-axis tilt angle, β, remains small is the main reason why off-axis coma can become important at resolutions approaching 0.4 nm. There are, in addition, two other ways in which off-axis coma is produced. Under typically used conditions, these additional contributions are small enough to be ignored, but nevertheless we briefly describe them here for completeness.

The first of these contributions is the radial coma that still remains when the β-angle, shown in Fig. 2C, is zero[5]. Such an effect is understandable when one recognizes that illumination that is parallel to the coma-free axis defined for one point in the specimen is necessarily tilted relative to the direction of the coma-free axis for a second point that is some distance from the (first) coma-free axis[6].

The second form of off-axis coma occurs because electrons follow spiral trajectories within the magnetic field of the lens. As a result, the incident illumination, which might have been expected to be parallel to the optical axis, is actually skewed (Christenson and Eades, 1986; Christenson and Eades, 1988), with the electron trajectories now being tilted azimuthally rather than radially. Like the angle β, the skew angle increases linearly with the distance from the coma-free axis. The resulting coma is referred to as azimuthal (anisotropic) coma, as its direction is tangential to a circle that could be drawn at a given radius.

[5] Slightly convergent illumination can actually produce zero radial off-axis coma (Rose, 2009). One can think of the radial off-axis coma introduced by using intentionally convergent illumination as compensating for the isotropic off-axis coma that exists for parallel illumination.

[6] For a thin lens, it is easy to see that a ray that passes through a point of the specimen that is at a position $\boldsymbol{R} \neq 0$ (relative to the current coma-free axis) is actually tilted by an angle $\sim R/f$ (where, f is the focal length of the lens) relative to the direction of the coma-free axis at the position $\boldsymbol{R} \neq 0$. For a thick lens, however, the radial coma that occurs at the position $\boldsymbol{R}$ is much smaller than would be expected, based on the angle calculated for a thin lens. This point emerges from ray tracing and/or calculation of the aberration integral.

4.2. When is off-axis coma important?

4.2.1. Effect due to convergent or divergent illumination

In order to understand when off-axis coma is important, we first consider the optics of the illumination system in more detail. In a two-condenser-lens system, the angle β shown in Fig. 2C, varies over the illuminated area by an amount that depends on the setting of C2. The condenser is said to be "in focus" when the cross-over is at the specimen. The cross-over then moves upwards or downwards when the condenser is over-focused or under-focused, respectively. When the condenser focus is changed sufficiently, the cross-over lies at the front focal plane of the objective-lens pre-field (see Footnote (8) for a further explanation of what is meant by "objective-lens pre-field"). As a result, the crossover (as seen by the specimen) reaches infinity, i.e. the illumination at the specimen is parallel. It must be emphasized that the beam thus is parallel across the field of view for only one specific value of the C2 lens. A more detailed description of the behavior of the β-angle beam tilt, which involves considering the virtual image of the C2 aperture as seen from the specimen plane, is presented in Fig. S2A[7] and Fig. S2B.

The maximum value of the beam tilt, $\beta_{\max}$, depends on the diameter D of the illuminated area as

$$\beta_{\max} = \frac{\left(\frac{D_{C2}}{M_{C2}} - D\right)}{2d}, \tag{5}$$

where, (as is indicated in Fig. S2) M_{C2} is the demagnification from the C2 aperture to the virtual image of the C2 aperture; D_{C2} is the diameter of the C2 aperture; and d is the distance from the specimen to the virtual image of the C2 aperture. The value of $\beta_{\max}$ varies linearly with D, the diameter of the illuminated area, as is shown in

[7] The images of the C2 aperture that are shown in Fig. S2A are referred to as virtual images. "Virtual" means that these are the images that would be formed if there were no magnetic field (and its associated lens action) below the specimen. The geometric construction of the virtual images of the C2 aperture shown in Fig. S2A is used to derive the linear relationship between β_{max} and D that is given in Eq. (5).

Fig. S3 for three sizes of the condenser aperture, and for the two modes (microprobe and nanoprobe, respectively) in which an FEI Twin objective lens can be used[8].

The amount of beam tilt, β_{max}, at the edge of a 1 μm-diameter field of illumination can easily be as much as 3 mrad, depending upon the size of the C2 aperture and other specific details of the illumination system, as can be seen from Fig. S3. The maximum value of the β-angle at the edge of the detector can be reduced by over-focusing C2 so that the beam extends well beyond the edge of the detector. This solution comes at the expense of decreasing the beam intensity and thus extending the exposures to what may become unacceptably long times. In addition, the user normally does not want the electron beam to irradiate as large an area of the specimen as is required to produce a sufficiently parallel electron beam within the field of the detector[9]. Instead, the incident beam is usually focused at a point above the specimen (C2 is then said to be "over-focused") that is just large enough to restrict the illumination to an area that is not much larger than the size of the detector. This means, unfortunately, that the illumination angle diverges over the field of view in the way that is shown in Fig. 2C (and in the third, i.e. middle, example in Fig. S2B).

As can be calculated from Eqs. (2) and (3), a beam-divergence angle, β, of 3 mrad will produce only a slight variation in defocus and astigmatism across the field of view when the electron energy is 300 keV, but at the edge of the field of view it causes the phases to be essentially random at a resolution better than ~0.6 nm. In order to keep the phase error less than 45° out to a resolution of 0.4 nm, on the other hand, the maximum value of β must be less than $\sim 8 \times 10^{-4}$ radians. A more detailed discussion is needed in order to specify the practical conditions, in terms of the C2 aperture size and the corresponding size of the illuminated area, for which off-axis coma remains small enough to avoid a significant phase error up to a resolution of ~0.4 nm. This discussion is taken up below, when we discuss various options for achieving nearly-isoplanatic imaging while, at the same time limiting the illuminated area to a size comparable to the area of the recorded image.

It is worth repeating that the beam is only truly parallel (apart from the "skew" due to spiral trajectories (Christenson and Eades, 1988)) over the whole field of illumination at one setting of the C2 lens, which corresponds to the beam being focused at the front focal plane of the upper objective pole piece (pre-field) lens. The pre-field lens is shown as a double-headed arrow in Fig. S2A, and the parallel illumination situation is indicated schematically in the fourth panel of Fig. S2B. When C2 is excited either more or less than this particular value, the illumination then begins to converge or diverge (at the specimen), respectively, as is indicated in Fig. S2B.

Whether there is a significant amount of off-axis beam tilt can sometimes, but not always, be evaluated by computing FFTs for small patches of the image at the edges of the detector and comparing these to the FFT of the same size of patch located at the center of the detector. An example of such a comparison is shown in Fig. 4. The microscope in this case was an FEI Tecnai 20 Twin operated at 120 keV. The C2 aperture used for this measurement was 100 μm in diameter, the C2 lens was adjusted to illuminate an area 0.8 μm in diameter, and the C1 lens excitation ("spot size") was adjusted to produce an exposure of 115 e/nm^2 during 1.0 s. The detector was a 4 × 4 k CCD camera and the magnification was chosen to make the pixel size on the CCD correspond to 0.1 nm at the specimen. As the various FFTs in Fig. 4 show, the amount of beam tilt, β, at the corners of the image is large enough to produce a just-barely detectable amount of astigmatism, and thus – necessarily – a large amount of off-axis coma, even though there is no significant axial coma. For single-particle cryo-EM images recorded under these conditions, the data quality at 0.4 nm resolution might be satisfactory for particles within the very central portion of the detector, but it would be useless for particles over the majority of the area of the detector.

4.2.2. Off-axis coma that remains when the illumination is parallel

The magnitude of the radial (isotropic) and azimuthal (anisotropic) coma that remains when the illumination is parallel to the (axial) coma-free axis has been calculated, as an example, for the specific case of the Tecnai 200 Twin objective lens (for an electron energy of 200 keV). The calculations were done in two different ways, using both ray tracing and numerical integration of the aberration integral[10], and the results obtained were very similar. We find that, at a position $\boldsymbol{R}$, the off-axis coma gives a phase error

$$\text{phase error} = 2\pi R\lambda^2 s^3[\tilde{K}_i(\hat{\boldsymbol{R}}\cdot\hat{\boldsymbol{s}}) + K_a(\hat{\boldsymbol{\varphi}}\cdot\hat{\boldsymbol{s}})] \quad (6)$$

in which the radial (isotropic) coma constant is $\tilde{K}_i = 0.06$, and the azimuthal coma constant is $K_a = 0.65$. The symbols $\hat{\boldsymbol{R}}, \hat{\boldsymbol{\varphi}}, \hat{\boldsymbol{s}}$ indicate unit vectors for the radial direction, the azimuthal direction, and the spatial frequency, respectively, and the tilde symbol on the isotropic coma constant indicates that it is the value for the specific case of parallel illumination. The phase error due to off-axis coma, for parallel illumination, is thus dominated by the effect of azimuthal coma. Furthermore, the radius beyond which the phase error at a resolution of 0.4 nm increases above 45° is, in the case of parallel illumination, equal to 2 μm.

While off-axis coma is thus not a major concern within the typically sized (~1 μm diameter) field of view, under parallel illumination conditions, it can become a concern when combined image shift and illumination shift are used to produce a series of images spanning a larger field of view. When using a software package for automated data collection, such as LEGINON (Potter et al., 1999; Suloway et al., 2005), it is useful to replace a physical movement of the stage by an equivalent shift of the image in order to move from one area to the next with greater accuracy and control, as well as to save the time that must normally be allowed for stage drift to stop after each movement of the stage. This feature is used routinely in experiments performed at the National Resource for Automated Molecular Microscopy (NRAMM), but the image

[8] Like in most present-day microscopes, the objective lens of the FEI Twin objective lens is a strong, symmetrical (or nearly symmetrical) magnetic lens of the condenser-objective type, where the specimen is placed approximately at the center of the lens. The magnetic field in front of the specimen, often referred to as the objective lens "pre-field" acts as a strong condenser lens with essentially the same focal length as the magnetic field below the specimen (which serves as the imaging part of the objective lens). In addition, a mini-lens is inserted into the upper pole piece. This additional lens, referred to as the condenser mini-lens, is usually operated in one of two modes, which in FEI instruments are referred to as the "microprobe" and "nanoprobe" modes, respectively. Switching between the microprobe and nanoprobe modes is accomplished by reversing the direction of the current of the condenser mini-lens. In the nanoprobe (or "off") mode the magnetic field in the gap of the mini-lens that is produced by the main (objective lens) coil is compensated by choosing the direction of the current in the mini-lens coil to be opposite to that of the main coil. In the microprobe (or "on") mode the directions of the currents in both coils are the same, thus producing a greater magnetic field in the gap of the condenser mini-lens.

[9] As was mentioned previously, the condition for producing parallel illumination across the entire field of view requires that the C2 lens is focused onto the front focal plane of the objective-lens pre-field. The illuminated area at the specimen then has the same size as the demagnified (virtual) image of the C2 aperture. For the Tecnai 200 Twin objective lens, this image is demagnified by a factor of ~5.2 in the microprobe mode and by a factor of ~40 in the nanoprobe mode. In general, the manufacturer's representative should be consulted to obtain the demagnification factor for other types of microscopes.

[10] As was indicated previously, the amount of off-axis coma that remains for a thick lens, when the illumination is parallel, cannot be accurately estimated from its focal length and spherical aberration constant, as can be done for a thin lens. As a result, the phase error due to off-axis coma must be represented in terms of two coma constants, one for the radial (isotropic) component and one for the azimuthal (anisotropic) component.

shift is typically limited to only ~0.7 μm, which is small enough that it does not, itself, generate significant off-axis coma.

4.3. What can be done to minimize off-axis coma?

4.3.1. Effect due to convergent or divergent illumination

Once the C2 lens excitation has been determined for which the β-angle is essentially zero (fourth example, Fig. S2B), the field of illumination at the specimen has the same size as the demagnified image of the C2 aperture. Adjusting the C2 lens excitation until the diameter of the illuminated area is equal to the C2 aperture diameter divided by the known demagnification factor is thus an especially convenient way to ensure that the illumination is focused at the front focal plane of the objective pre-field lens. As we mentioned in Footnote (9), the demagnification in the image of the C2 aperture that is produced in the microprobe and nanoprobe modes of the Tecnai 200 Twin objective lens is approximately 5.2× and 40×, respectively.

One might thus suppose that the nanoprobe mode is preferred if one wants to limit the size of the area that is illuminated. Even so, the diameter of the illuminated area may still be larger than most users have been accustomed to use. In order to limit a parallel beam of illumination to an area that is smaller than 1 μm in diameter, for example, even when using the nanoprobe mode, it is necessary to use a C2 aperture that is smaller than 40 μm in diameter. It is also important to emphasize how precisely the beam must be focused onto the front focal plane of the objective-lens pre-field is much more critical in the nanoprobe mode than it is in the microprobe mode. This fact can be appreciated from the relatively steep slope of the graphs of β angle vs. diameter of the illuminated area that are presented in Figs. S3A (microprobe) and S3B (nanoprobe), respectively.

Similar modes are available for any electron microscope that is equipped with a so-called condenser mini-lens. In addition, a few types of electron microscope, such as the Zeiss Libra or the FEI Titan, have three rather than two continuously adjustable condenser lenses. The additional degree of freedom provided by a third condenser lens makes it possible to keep the illumination parallel while the diameter of the illuminated area (i.e. the demagnification factor) is varied continuously (“zoomed”) over a wide range. Since the demagnification factor depends greatly on the type of microscope, users must consult the manufacturer to know what the factor is for their particular type of instrument.

4.3.2. Off-axis coma that remains when using parallel illumination

As was mentioned in Footnote (5), isotropic coma can actually be reduced to zero by using slightly convergent illumination rather than perfectly parallel illumination. In this case the isotropic coma that is due to the (convergent) β angle is opposite in direction to that which remains when the illumination is parallel to the (axial) coma-free axis. Since the azimuthal coma is significantly larger than the isotropic coma, however, it is hardly worth the effort to optimize the β angle more precisely than to simply set it equal to zero.

Off-axis coma can, in principle, be avoided by combining parallel illumination of a relatively small area, deflection of the beam to successive positions, and dynamic adjustment of the tilt angle at each new position. This same approach was used previously by Eades to maintain a fixed orientation of the beam relative to the specimen over extended areas of a thin crystal (Eades, 2006). The concept in our case is to ensure that both the isotropic and anisotropic coma can be ignored within any one spot, regardless of its position. We emphasize that dynamic compensation for the position-dependence of coma should not be required if data are to be collected from positions that are only ~2 μm or less from the coma-free axis, but that it is likely to be useful for automated data collection covering much larger areas.

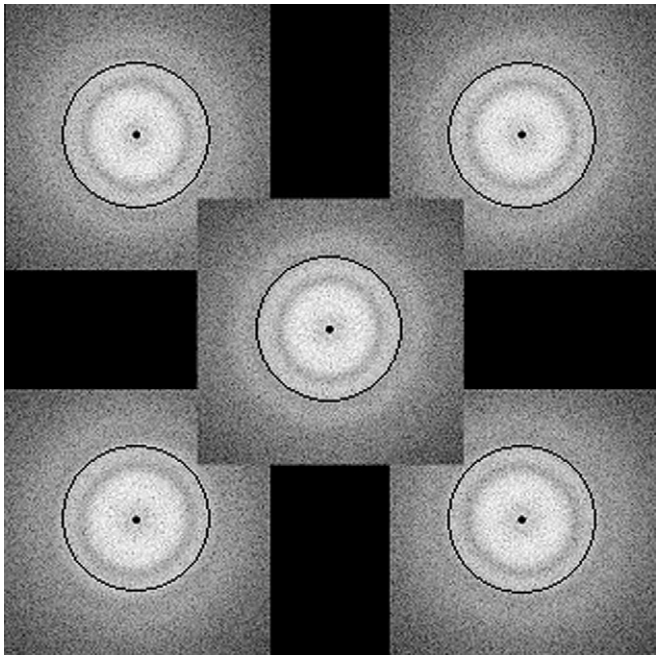

Fig. 4. Tableau of FFTs obtained from 50.1 × 50.1 nm areas at the corners and at the center of an image recorded with a 4 × 4 k CCD camera. The distance between the center and any given corner image is 248 nm. Details of the conditions under which the image was recorded are given in the text. Although the image at the center of the camera is coma-free, there is still sufficient off-axis coma to produce a barely detectable difference in focus and astigmatism at the corners of the detector relative to that at the center of the detector. The off-axis coma is due in this case to the large beam-divergence angle, β, that occurs under the “standard imaging conditions” described in the text. Although the change in defocus and astigmatism at the corners of the detector is barely detectable, it is important to emphasize that detecting even this very small effect is sufficient to tell one that the underlying variation in beam tilt across the field of view produces an unacceptably large amount of off-axis coma at a resolution of 0.4 nm.

5. Practical examples of conditions that provide nearly-isoplanatic images

In this section we examine more closely the question of how – for a given C2 aperture size – the size, D, to which the illumination is spread (by varying the excitation of the C2 lens) affects the amount of coma that is present within the field of view. What we mean by the expression “nearly isoplanatic” in this section is that off-axis coma does not introduce a phase error larger than 45° at a given resolution, which we assume to be 0.4 nm in our examples below. Since a phase error of 45° is actually much larger than one would normally wish to have, our examples should be considered to be the “worst that one could accept”. Users should themselves use these examples as a guide on how to calculate the illumination conditions that can provide an even smaller phase error.

As previously, we consider the case that there are only two user-adjustable condenser lenses, but that there is also a condenser mini-lens that can be switched either “on” or “off” (see Footnote (8)). Numerical examples are then presented for the specific case of an FEI Tecnai 200 Twin objective lens.

5.1. Representation of isotropic coma by an illumination-dependent coma constant

In a similar way to equations 4 and 6, the phase error due to radial coma can be written as

$$\text{Phase error} = 2\pi\lambda^2 s^3(\beta+\beta')C_s(\hat{\boldsymbol{R}}\cdot\hat{\boldsymbol{s}}). \tag{7}$$

The angle β is, as before, the beam tilt at radius R due to divergent (or convergent) illumination[11], while β' is the rather small, convergent angle discussed previously (e.g. Footnote (5)), at which the radial component of the off-axis coma vanishes. As before, $\hat{\boldsymbol{R}}$ and $\hat{\boldsymbol{s}}$ are unit vectors in real and reciprocal space, respectively.

We use the information about the longitudinal position of the focused spot of the illumination as well as the size and the longitudinal position of the demagnified (virtual) image of the C2 aperture (see middle example, Fig. S2B) to determine how the angle β, and thus the off-axis coma, depends on the size, D, of the illuminated area. The angle β can be expressed by the radius R and the distance d_S of the virtual source from the specimen plane: $\beta = R/d_S$. Using the geometrical relation between the diameter of the illuminated specimen area and the virtual image of the C2 aperture (see Fig. S2B), $1/d_S$ can be expressed by

$$\frac{1}{d_S} = \frac{D_{C2}/M_{C2} - D}{D \times d}. \tag{8}$$

As before, D_{C2} is the diameter of the condenser aperture, M_{C2} is the demagnification factor, D is the diameter of the illuminated area, and d is the distance of the virtual image of the C2 aperture from the specimen plane. Comparing Eqs. (8) and (6) one gets for the isotropic coma constant K_i:

$$K_i = C_s/d_S = C_s \times \frac{D_{C2}/M_{C2} - D}{D \times d} + \tilde{K}_i, \tag{9}$$

where, $\tilde{K}_i$ is the coma constant for parallel illumination that was mentioned in Eq. (6). As one would expect, it follows from Eq. (9) that K_i becomes infinite when the diameter of the illuminated area goes toward zero, i.e. when the spot is focused at the specimen.

5.2. Complete representation of coma, assuming that axial coma has been corrected perfectly

To obtain the combined off-axis coma constant[12], K, one has to add the radial (isotropic) and azimuthal constants quadratically, i.e.

$$K = \sqrt{K_i^2 + K_a^2}, \tag{10}$$

since the directions for the two effects are perpendicular to one another. The dependence of the combined coma constant, K, on the diameter of the illuminated area for the microprobe mode is shown in Figs. S4A and S4B for the case that C2 is over-focused or under-focused, respectively, using the parameters $M_{C2} = 5.2$, $d = 3.4$ mm, and $C_s = 2.2$ mm. Figs. S4C and S4D show the corresponding dependence for the nanoprobe mode for the case that C2 Is under-focused or over-focused, respectively, using $M_{C2} = 40$ and $d = -85$ μm. All curves start at a high value, but the curves go through a minimum when C2 is over-focused in the microprobe mode and when C2 is under-focused in nanoprobe, in which case the radial coma becomes zero and thus only the azimuthal coma contributes.

5.3. Calculation of the diameter of the nearly-isoplanatic area

In order to define the illumination conditions that are suitable for data collection at an intended resolution, we compare the diameter, $2R_{max}$, of the useful (nearly-isoplanatic) region with that of the illuminated area. One obtains

$$\frac{2R_{max}}{D} = \frac{1}{4D\lambda^2 s_{max}^3 K}, \tag{11}$$

where K is obtained from equation 10, substituting the right hand side of Eq. (9) for K_i and using our calculated value of 0.65 for K_a. It is important to note that the size of the nearly-isoplanatic region depends strongly on the intended resolution, which is expressed in Eq. (11) as the maximum spatial frequency.

Plots of the ratio $2R_{max}/D$ are shown in Fig. 5 for representative values of the diameter of the C2 aperture, assuming a resolution limit of 0.4 nm. Values of this ratio for 300 keV electrons are shown in panels A and B, while values for 120 keV electrons are shown in panels C and D. Values of this ratio for the microprobe mode are shown in panels A and C, and values for the nanoprobe mode are shown in panels B and D. While numerical values of the ratio greater than 1.0 have no practical significance (since one does not collect image data at a radius larger than that of the illuminated area), a partial continuation of the curves to values larger than 1.0 is nevertheless shown (in the shaded area) just to give a more complete impression of the mathematical behavior of the curves.

What is important when considering the curves in Fig. 5 is that one should avoid using illumination conditions for which the ratio $2R_{max}/D$ is smaller than 1. This point is especially true if one does not want the size, D, of the illuminated area to be much larger than the field of view of the detector (CCD camera or film), as is usually the case for cryo-EM data collection. In any case, one must ensure that the values of the β angle within the field of view of the detector are small enough to keep the phase error due to off-axis coma to an acceptably small value at the resolution of interest. As a rule of thumb, for example, if one uses one of the illumination conditions shown in Fig. 5 for which $2R_{max}/D < 1.0$, then the phase error at a resolution of 0.4 nm will be greater than 45° for the outer annulus of the illuminated area, corresponding to $R_{max} < R < D/2$.

Another significant point that is contained in the curves shown in Fig. 5A is the fact that off-axis coma can be unimportant at 300 keV if one uses a C2 aperture that is 30–40 μm in diameter. At an energy of 120 keV, however, the aperture must be even smaller, for example 10–20 μm in diameter, as is shown in Fig. 5C. As long as one has properly adjusted the beam-tilt angle, θ, to achieve (axial) coma-free alignment, the images will then be essentially coma-free over the entire field of view, for almost any size of illuminated area. On the other hand, with a C2 aperture that is 50 μm or larger, one can only realize good illumination conditions in the microprobe mode at the expense of illuminating a much larger area than one would normally be willing to use.

Finally, when optimizing the illumination, one has to take into account that the intensity may become very low for near-isoplanatic illumination conditions in the microprobe mode. As a result, the exposure times may well become considerably longer than 10 s, especially if something like a 10 μm diameter C2 aperture is used. One must also take into consideration the fact that the allowed illumination conditions become even more restrictive[13] as the intended resolution increases even further, for example to ~0.3 nm. Rather than using a very small C2 aperture in the microprobe mode, it may become advisable to choose the nanoprobe (or equivalent) mode, taking care to use the appropriate size of C2 aperture to match the diameter of the detector (CCD camera or film). The advantage of the nanoprobe mode in this case is that it produces greater intensity within the illuminated area, due to the greater demagnification of the virtual image of the C2 aperture.

[11] The angle β is considered to be positive for divergent illumination and negative for convergent illumination.

[12] Rose (2009) uses the notation K_3 for the off-axis (third-order) coma constant. For the radial and azimuthal coma constants he uses the notation K_{3r} and K_{3i}, respectively.

[13] The reader can use Eq. (11) to compute curves similar to those shown in Fig. 5 for a range of C2 aperture sizes in order to define the combination of C2 aperture size and size of illuminated area that apply to their particular electron microscope, perhaps with a mini-condenser lens in both the "on" and "off" setting, such that nearly-isoplanatic imaging is achieved at the desired target resolution.

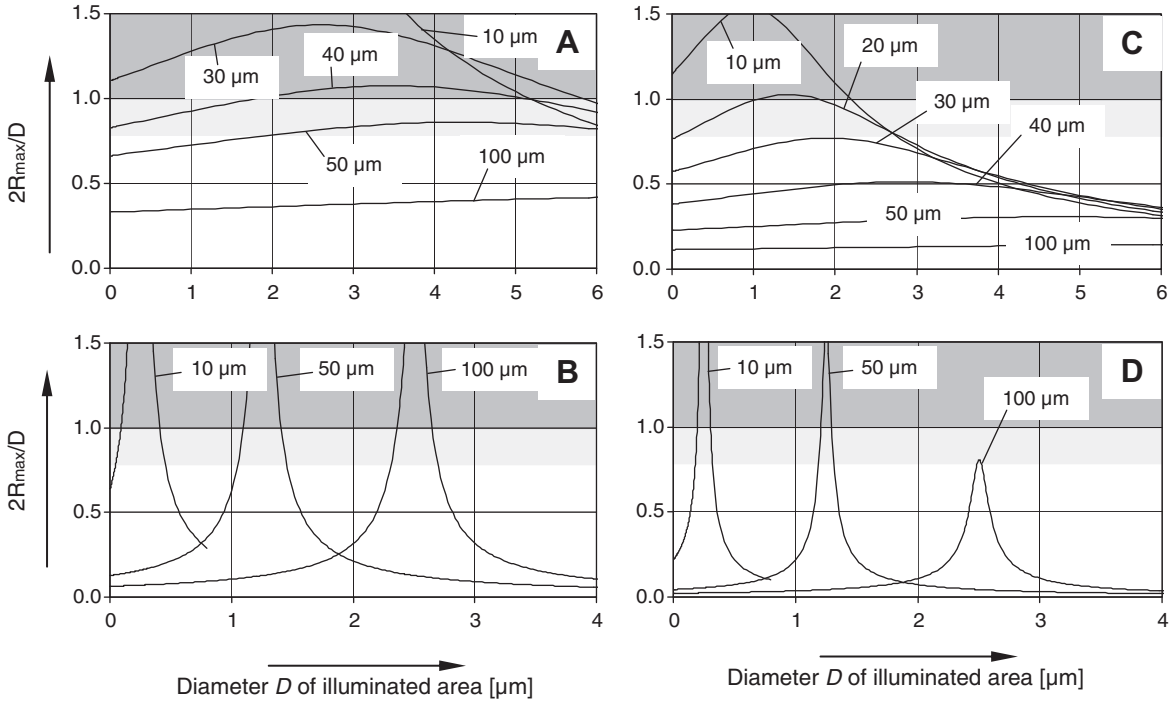

Fig. 5. Graphs of the ratio, $2R_{max}/D$, of the diameter of the nearly-isoplanatic area to the diameter of the illuminated area. While it is often desirable to condense the beam to a size that is only slightly larger than the field of view recorded on the detector, $2R_{max}/D$ must not be allowed to fall much below 1.0. Regions of the graph for which the ratio is less than or equal to 1 are thus shown without shading, to draw the reader's attention to the extent to which the conditions of illumination become less and less acceptable as one varies the diameter of the illuminated area for a given size of C2 aperture. On the other hand, since values of the ratio greater than 1 imply that the diameter of the nearly-isoplanatic area is larger than that over which data can be collected (i.e. the illuminated area), this portion of the graph is shown in grey, to emphasize that the actual values of the ratio no longer matter. Nevertheless, short portions of the curves are shown in this region, just to give a feeling for their mathematical behavior. At the same time, the reader should realize that the acceptable conditions, for which the ratio is greater than 1, become increasingly restricted as the resolution increases. As an example, the curves shown here represent only the case when one is willing to accept phase errors (at a resolution of 0.4 nm) of 45° at positions close to the edge of the illuminated area. (A) Microprobe mode, 300 keV. (B) Nanoprobe mode, 300 keV. (C) Microprobe mode, 120 keV. (D) Nanoprobe mode, 120 keV.

6. Summary

When the illumination is tilted relative to the (coma free) optical axis, an azimuthally varying phase error is introduced in the estimated structure factors that are derived (for weak phase objects) from the computed Fourier transform of the image intensity. It is important to recognize that this phase error is not reduced by applying the usual CTF correction. As a result, it is desirable to ensure that the amount of beam tilt is small enough that the phase error is negligible. Since the value of this phase error increases as the cube of the resolution, it is necessary to pay much greater attention to both proper beam alignment and proper beam collimation when aiming for a resolution of ~0.4 nm or better than is required when aiming for a resolution of ~0.8 nm. If the field of view of the detector is small enough that one can ignore the off-axis coma that occurs for parallel illumination, one must still take care (1) that the illumination is sufficiently parallel to the coma-free axis and (2) that the illumination is sufficiently parallel across the field of view. The first condition is conveniently satisfied by using a coma-free alignment procedure, but the latter is satisfied only when the illumination is focused close to the front focal plane of the pre-field of the (upper) objective-lens pole piece.

Acknowledgments

We thank Dr. Bridget Carragher and Dr. Clint Potter for encouraging the preliminary experiments that ultimately led to writing this review. This work has been supported in part by NIH Grant GM083039, NIH Grant RR175732, and US Department of Energy contract DE-AC02-05CH11231.

Appendix A. Supplementary data

Supplementary data associated with this article can be found, in the online version, at doi:10.1016/j.jsb.2010.12.005.

References

Chen, J.Z., Settembre, E.C., Aoki, S.T., Zhang, X., Bellamy, A.R., Dormitzer, P.R., Harrison, S.C., Grigorieff, N., 2009. Molecular interactions in rotavirus assembly and uncoating seen by high-resolution cryo-EM. Proceedings of the National Academy of Sciences of the United States of America 106, 10644–10648.

Christenson, K.K., Eades, J.A., 1986. On parallel illumination in the transmission electron microscope. Ultramicroscopy 19, 191–194.

Christenson, K.K., Eades, J.A., 1988. Skew thoughts on parallelism. Ultramicroscopy 26, 113–132.

Cong, Y., Baker, M.L., Jakana, J., Woolford, D., Miller, E.J., Reissmann, S., Kumar, R.N., Redding-Johanson, A.M., Batth, T.S., Mukhopadhyay, A., Ludtke, S.J., Frydman, J., Chiu, W., 2010. 4.0 Å resolution cryo-EM structure of the mammalian chaperonin TRiC/CCT reveals its unique subunit arrangement. Proceedings of the National Academy of Sciences of the United States of America 107, 4967–4972.

Eades, A., 2006. Obtaining TEM images with a uniform deviation parameter. Ultramicroscopy 106, 432–438.

Fernandez, J.J., Luque, D., Caston, J.R., Carrascosa, J.L., 2008. Sharpening high resolution information in single particle electron cryomicroscopy. Journal of Structural Biology 164, 170–175.

Frank, J., 1973. Envelope of electron-microscopic transfer-functions for partially coherent illumination. Optik 38, 519–536.

Frank, J., 2006. Three-Dimensional Electron Microscopy of Macromolecular Assemblies – Visualization of Biological Molecules in Their Native State, second ed. Oxford University Press, New York.

Glaeser, R.M., Downing, K., DeRosier, D., Chiu, W., Frank, J., 2007. Electron Crystallography of Biological Macromolecules. Oxford University Press.

Henderson, R., Glaeser, R.M., 1985. Quantitative-analysis of image-contrast in electron-micrographs of beam-sensitive crystals. Ultramicroscopy 16, 139–150.

Henderson, R., Baldwin, J.M., Downing, K.H., Lepault, J., Zemlin, F., 1986. Structure of purple membrane from halobacterium-halobium – recording, measurement

and evaluation of electron-micrographs at 3.5 Å resolution. Ultramicroscopy 19, 147–178.
Jiang, W., Baker, M.L., Jakana, J., Weigele, P.R., King, J., Chiu, W., 2008. Backbone structure of the infectious epsilon 15 virus capsid revealed by electron cryomicroscopy. Nature 451, 1130–1134.
Koster, A.J., de Ruijter, W.J., 1992. Practical autoalignment of transmission electron microscopes. Ultramicroscopy 40, 89–107.
Ludtke, S.J., Baker, M.L., Chen, D.H., Song, J.L., Chuang, D.T., Chiu, W., 2008. De novo backbone trace of GroEL from single particle electron cryomicroscopy. Structure 16, 441–448.
Potter, C.S., Chu, H., Frey, B., Green, C., Kisseberth, N., Madden, T.J., Miller, K.L., Nahrstedt, K., Pulokas, J., Reilein, A., Tcheng, D., Weber, D., Carragher, B., 1999. Leginon: a system for fully automated acquisition of 1000 electron micrographs a day. Ultramicroscopy 77, 153–161.
Rose, H.H., 2009. Geometrical Charged-Particle Optics. Springer, Berlin.
Smith, D.J., Saxton, W.O., Okeefe, M.A., Wood, G.J., Stobbs, W.M., 1983. The importance of beam alignment and crystal tilt in high-resolution electron-microscopy. Ultramicroscopy 11, 263–281.
Suloway, C., Pulokas, J., Fellmann, D., Cheng, A., Guerra, F., Quispe, J., Stagg, S., Potter, C.S., Carragher, B., 2005. Automated molecular microscopy: the new Leginon system. Journal of Structural Biology 151, 41–60.
Typke, D., Dierksen, K., 1995. Determination of image aberrations in high-resolution electron microscopy using diffractogram and cross-correlation methods. Optik 99, 155–166.
Typke, D., Gilpin, C.J., Downing, K.H., Glaeser, R.M., 2007. Stroboscopic image capture: reducing the dose per frame by a factor of 30 does not prevent beam-induced specimen movement in paraffin. Ultramicroscopy 107, 106–115.
Wade, R.H., Frank, J., 1977. Electron-microscope transfer-functions for partially coherent axial illumination and chromatic defocus spread. Optik 49, 81–92.
Wolf, M., Garcea, R.L., Grigorieff, N., Harrison, S.C., 2010. Subunit interactions in bovine papillomavirus. Proceedings of the National Academy of Sciences of the United States of America 107, 6298–6303.
Yu, X.K., Jin, L., Zhou, Z.H., 2008. 3.88 Å Structure of cytoplasmic polyhedrosis virus by cryo-electron microscopy. Nature 453, 415–419.
Zemlin, F., Weiss, K., Schiske, P., Kunath, W., Herrmann, K.H., 1978. Coma-free alignment of high-resolution electron-microscopes with aid of optical diffractograms. Ultramicroscopy 3, 49–60.
Zhang, X., Jin, L., Fang, Q., Hui, W.H., Zhou, Z.H., 2010. 3.3 Angstrom cryo-EM structure of a nonenveloped virus reveals a priming mechanism for cell entry. Cell 141, 472–482.
Zhang, X., Settembre, E., Xu, C., Dormitzer, P.R., Bellamy, R., Harrison, S.C., Grigorieff, N., 2008. Near-atomic resolution using electron cryomicroscopy and single-particle reconstruction. Proceedings of the National Academy of Sciences of the United States of America 105, 1867–1872.
Zhou, Z.H., 2008. Towards atomic resolution structural determination by single-particle cryo-electron microscopy. Current Opinion in Structural Biology 18, 218–228.